Individual addressing in quantum computation through spatial refocusing

C. Shen,[1,2,*] Z.-X. Gong,[1,3] and L.-M. Duan[1,2]

[1]*Department of Physics, University of Michigan, Ann Arbor, Michigan 48109, USA*
[2]*Center for Quantum Information, IIIS, Tsinghua University, Beijing, China*
[3]*Joint Quantum Institute, University of Maryland, College Park, Maryland 20742, USA*

Separate addressing of individual qubits is a challenging requirement for scalable quantum computation, and crosstalk between operations on neighboring qubits remains a significant source of error for current experimental implementations of multiqubit platforms. We propose a scheme based on spatial refocusing from interference of several coherent laser beams to significantly reduce the crosstalk error for any type of quantum gate. A general framework is developed for the spatial refocusing technique, in particular with practical Gaussian beams, and we show that the crosstalk-induced infidelity of quantum gates can be reduced by several orders of magnitude with a moderate cost of a few correction laser beams under typical experimental conditions.

I. INTRODUCTION

Performing useful quantum computation and simulation in the presence of unavoidable noise has been a goal long sought after. Many solid steps have been taken on different physical platforms in the past decade, demonstrating for small systems elementary quantum logic [1], simple algorithms [2], error correction [3], and quantum simulation [4]. While the celebrated error threshold theorem [5] guarantees the fault tolerance of a large-scale quantum computer when each single operation error is reduced below a certain limit, this threshold is very hard to satisfy in a typical multiqubit setting. To fully control the state evolution of the quantum-information processor, one needs to pinpoint any individual qubit at will and manipulate it while keeping the others intact. This is a stringent requirement for almost all physical platforms. A lot of efforts have been devoted to the development of individual addressing optical beam delivery and imaging systems [6,7]. Assuming a Gaussian profile of the beam, single-qubit addressing typically requires the beam waist to be much smaller than the interqubit spacing, which is half the wavelength of the trapping laser in optical lattices and around $1\,\mu$m in a linear trapped ion chain. So subwavelength focusing beyond the diffraction limit is usually required and this makes it experimentally very challenging.

There have already been many proposals and/or demonstrations in the context of cold atoms in optical lattices [8–11] and linearly trapped ions [12,13]. To name a few, interference of several Bessel beams were proposed to form a pattern such that all but one atom locate at the nodes of laser profile [8]; the sharp nonlinear atomic response and position-dependent dark states in an electromagnetically induced transparency (EIT) setting were exploited to enable subwavelength selectivity in various proposals [9] and experimentally demonstrated very recently [10]; single spin manipulation in an optical lattice with the combination of a well-focused level shifting beam and a microwave pulse has also been demonstrated [11]. The adaptation of the composite pulse refocusing technique widely used in nuclear magnetic resonance [14] and quantum

information [15] to trapped ions was considered for single-qubit operation [12] and two-qubit operation with a special form of interaction [13]. Note the two-qubit correction scheme depends on the physical operation being carried out and requires a specific form of controllable interaction, and does not reduce error for certain gate realizations.

Our approach is along the line of Ref. [8] but in a different setting. We propose and provide detailed analysis for a scheme to reduce crosstalk error and achieve individual addressing with several imperfectly focused laser beams. By applying an array of beams centered at different qubits and controlling their relative amplitudes, we can achieve quantum gates with ideal fidelity even when the beam waist is comparable with or slightly larger than the interqubit distance. A reduction of the crosstalk error by several orders of magnitude can be achieved with only a moderate increase of the required laser power. The basic idea is reminiscent of the refocusing in NMR, but works in the spatial domain using multiple beams instead of in the time domain. So we call this technique spatial refocusing. Unlike the technique in Ref. [13], this technique is universal and works for any quantum gate. We believe it is a valuable addition to the existing toolbox of subwavelength addressing.

II. MATHEMATICAL FORMULATION

We consider an array of qubits with even spacing a located at the positions x_i $(i = 1, 2, \ldots, N)$. The laser beam used to manipulate the qubits is assumed to have a spatial profile denoted by $g(x - x_i)$ when it is centered at x_i. To have individual addressing, normally we assume the laser is strongly focused so that $g(x_j - x_i) \to 0$ for any $j \neq i$ [i.e., $g(x_j - x_i) = \delta_{ij}$]. It remains experimentally challenging to achieve this condition in multiqubit quantum computing platforms where the spacing a needs to be small to have sufficiently strong interaction. Here, instead of strong focusing, we assume that the laser beams applied to different qubits have relative coherence. To address a single qubit, say qubit i at position x_i, instead of just shining this qubit with $g(x - x_i)$, we apply a number of identical beams centered on its nearby qubits with relative amplitudes denoted by $f(x_j - x_i)$. The total effective

_____
*chaoshen@umich.edu

laser profile is then the convolution

$$G(x - x_i) = \sum_j g(x - x_j) f(x_j - x_i). \tag{1}$$

For a given $g(x - x_i)$, we want to find an envelop function $f(x_j - x_i)$ to make $G(x_j - x_i) \to 0$ for any $j \neq i$. It is desirable that $f(x_j - x_i)$ is fast decaying so that in practice we can cut off j in the summation of Eq. (1) and apply laser beams to only a few of its neighbors. If we take the normalization $g(0) = G(0) = 1$, $f(0)$ then determines the relative increase of the required laser light amplitude, which is desired to be moderate for practical applications.

The solution depends on the laser profile $g(x - x_i)$. To show that the idea works, first we look at a toy model by assuming $g(x - x_i)$ given by an exponential decay $g(x - x_i) = e^{-\alpha|x - x_i|}$. In this case, two correction beams applied to its nearest neighbors x_{i-1} and x_{i+1} perfectly cancel the residue laser amplitude for all the qubits $j \neq i$. To see this, let us take $f(0) = \beta_0$, $f(x_j - x_i) = \beta_1$ for $j = i \pm 1$, and all other $f(x_j - x_i) = 0$. If we choose $\beta_0 = (1 + \lambda^2)/(1 - \lambda^2)$ and $\beta_1 = -\lambda/(1 - \lambda^2)$, where $\lambda \equiv e^{-\alpha a}$, we immediately have $G(x_j - x_i) = \delta_{ij}$. The required increase of the laser power $f(0) = (1 + \lambda^2)/(1 - \lambda^2)$ is moderate even when the original laser profile $g(x - x_i)$ has a significant residue amplitude $\lambda = e^{-\alpha a}$ on the neighboring qubits.

For a general laser profile $g(x - x_i)$, if the number of qubits is large or if the envelop function $f(x_i)$ is fast decaying so that the boundary condition is irrelevant, we can formally solve Eq. (1) by assuming the periodic boundary condition for the array. In this case, we can take a discrete Fourier transformation of Eq. (1), which yields $g(k) f(k) = G(k)$. Because the target profile $G(x - x_i)$ needs to be a δ function, $G(k) = 1$, and a formal solution of Eq. (1) is

$$f(x_j - x_i) = \frac{1}{N} \sum_k \frac{1}{g(k)} e^{ik(x_j - x_i)/a}, \tag{2}$$

where the summation is over $k = \pi n / N$ with $n = -N/2$, $-N/2 + 1, \ldots, N/2$. In the limit of large N, $f(x_j - x_i) \approx (1/2\pi) \int_{-\pi}^{\pi} dk [1/g(k)] e^{ik(x_j - x_i)/a}$.

Now we apply this formalism to practical Gaussian beams, for which $g(x - x_i) = \exp[-(x - x_i)^2/w^2]$, where w characterizes the width of the beam. The discrete Fourier transformation of $g(x - x_i)$ gives

$$g(k) = \sum_{n \in Z} \exp[-(na)^2/w^2] \exp(-ikn) = \theta_3(k/2, \gamma), \tag{3}$$

where $\gamma \equiv e^{-a^2/w^2} < 1$ and $\theta_3(z, q) \equiv 1 + 2\sum_{n=1}^{\infty} q^{n^2} \cos(2nz)$ is the Jacobi elliptic function. We can do a series expansion with γ, and up to the order of γ^2, $g(k) \approx 1 + 2\gamma \cos(k) + O(\gamma^4)$ and $f(x_j - x_i) \approx (1 + 2\gamma^2)\delta_{ij} - \gamma\delta_{i\pm1,j} + \gamma^2\delta_{i\pm2,j}$. One can see that the envelop function $f(x_j - x_i)$ decays exponentially by the factor $-\gamma$ as one moves away from the target qubit. This result holds in general. To show this, we write Eq. (1) into a matrix form, $\sum_j M_{nj} f_{ji} = \delta_{n,i}$, denoting x as $x_n = na$ and $g(x_n - x_j)$ as $M_{nj} = e^{-(n-j)^2 a^2/w^2} = \gamma^{(n-j)^2}$, where n and j are integers between 1 and N. For large enough positive integers m, $\gamma^m \ll 1$, so we can always cut off at certain m and set terms $O(\gamma^{m+1})$ in M_{nj} to zero. The
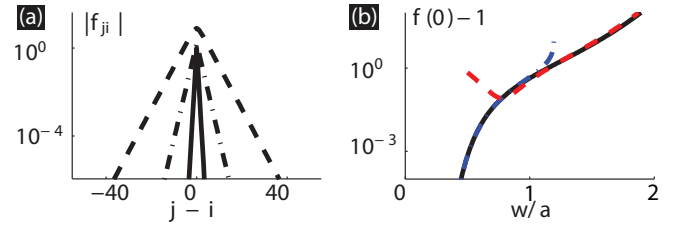

FIG. 1. (Color online) (a) Envelope function f_{ji} under different Gaussian beam waist ($w/a = 1.5$, 1.0, and 0.5 for curves from top to bottom), calculated for a homogeneous chain of 401 qubits. Near the center $j - i = 0$, f_{ji} has coexisting components with different decay constants so $|f_{ji}| = (-1)^{j-i} f_{ji}$ deviates from a straight line on the log plot. Only a few lattice sites away, $|f_{ji}|$ straightens and the slope matches that of $\gamma^{|j-i|}$ precisely. (b) Amplitude $f(0)$ versus the beam waist w/a. For visibility $f(0) - 1$ is plotted. The black solid line is from the numerical exact integration of Eq. (2) and the blue dash-dot (red dashed) line is from the analytic approximation $f(0) = 1/\sqrt{1 - 4\gamma^2}$ [$f(0) = \frac{2}{\pi^{5/2} w^3} e^{\pi^2 w^2/4}$], valid for the region $w/a \lesssim 1$ ($w/a \gtrsim 1$).

resulting M_{nj} is then a Toeplitz band matrix with bandwidth $2m + 1$ [16]. The solution f_{ji} contains several exponential decay components with different decay constants (see the Appendix for details), but $|-\gamma|$ characterizes the largest decay constant and in the limit of large $|j - i|$ a single term wins out with $f_{ji} \equiv f(x_j - x_i) \sim (-\gamma)^{|j-i|}$. Numerical solution of the matrix equation confirms this [see Fig. 1(a)]. An important implication of this result is that we can set a truncation tolerance error ϵ and only apply correction beams to those qubits with $|f_{ji}| > \epsilon$. This will require about $2 \ln \epsilon / \ln \gamma = 2(w/a)^2 \ln(1/\epsilon)$ beams, independent of the system size. We expect this qualitative behavior to persist for any beam profile that decays quickly with the increase of distance from its center.

The amplitude $f(0)$, characterizing the required laser power, is plotted in Fig. 1(b) as a function of w/a from the exact numerical solution of Eq. (1). When $w/a \lesssim 1$, γ is small, and from a truncation of Eq. (2) $g(k) \approx 1 + 2\gamma \cos(k)$, we find $f(0) \approx (1/2\pi) \int_{-\pi}^{\pi} dk [1/g(k)] \approx 1/\sqrt{1 - 4\gamma^2}$. In the other region with $w/a \gtrsim 1$, the summation in Eq. (3) can be approximated with an integration, which yields $g(k) \approx \sqrt{\pi w^2/a^2} e^{-k^2 w^2/(4a^2)}$ and therefore $f(0) \approx \frac{2a^3}{\pi^{5/2} w^3} e^{\pi^2 w^2/(4a^2)}$. These two analytic expressions, also drawn in Fig. 1(b), agree well with the exact solution in their respective regions. Note that for $w/a \lesssim 1$, $f(0)$ is close to unity and the cost in laser power in negligible. For $w/a \gtrsim 1$, $f(0)$ increases exponentially with w^2/a^2, and the scheme becomes impractical when $w^2/a^2 \gg 1$. Our scheme is most effective in the region $w/a \sim 1$, where it allows a reduction of the crosstalk error by several orders of magnitude with just a few correction beams while keeping the cost in laser power still negligible.

The above analysis extends straightforwardly to higher-dimensional systems. Moreover, neither the assumption of homogeneous spacing nor that correction beams center around each qubit is essential. We can always treat the qubits as equidistant if we effectively modify the beam profile $g(x - x_i)$ or M_{nj} according to the actual qubit spacings and the focus positions of the correction lasers.

For multiqubit operations, the relative overhead of spatial refocusing usually becomes lower. For instance, in Ref. [17] the quantum simulation of the arbitrary Ising interaction with N trapped ion qubits requires N^2 well-focused laser beams. Without perfect focusing, using the scheme here we still only need N^2 beams.

III. SPECTRAL REFOCUSING

Instead of using localized beams, an alternative for spatial refocusing is to spectrally decompose the desired amplitude profile and use broad beams of traveling plane waves with varying wave vectors k to reconstruct a focused beam. Note here we do not use light beams with different frequencies. We simply tilt the traveling wave direction so that the effective spatial periodicity is varied along the system axis. The desired spatial profile $G(x_j - x_i) = \delta_{ij}$, transformed to the momentum space, is a constant function. For N qubits, one can use N plane waves with k evenly spread in the Brillouin zone $[-\pi/a, \pi/a]$ to reconstruct the profile δ_{ij}. We may tilt a traveling wave with a fixed k by different angles with respect to the qubit array to get a varying wave-vector component k_x along the axis. For ion qubits in a harmonic trap, the spacing is inhomogeneous and the exact amplitudes of the components are not even, but can be obtained using the matrix formalism of Eq. (1). For the plane wave with wave vector k_x^j, the amplitude at position x_n is $M_{nj} = \exp(i\,k_x^j\,x_n)$. To get a perfectly focused beam at position x_i, the amplitude f_{ji} for the k_x^j component is given by the solution of the matrix equation $\sum_j M_{nj} f_{ji} = \delta_{ni}$. The maximum $k_x^j = k\sin(\theta_m)$ needs to be comparable with π/a, so we require the laser angle be tunable over a window $[-\theta_m, \theta_m]$, where $\theta_m \approx \sin(\theta_m) \approx \pi/ka$ is typically small. For instance, in an ion trap quantum computer, the ion spacing is about 5 μm and the laser has a wavelength of about 0.4 μm, which gives $\theta_m \sim 0.04 \sim 2.3°$. In Fig. 2(a), we show the amplitude distribution $f(k_x^j)$ for 21 ions in a harmonic trap and the associated profile $G(x)$, which is basically a δ function at ions' positions albeit with small wiggles at other locations. This spectral decomposition approach is particularly convenient for quantum simulation where we need to simultaneously apply focused laser beams on each ion [17]. With spectral decomposition, we only need to apply a number of broad plane wave beams that cover all the ions, with their angles tunable in a small window $[-\theta_m, \theta_m]$.

IV. APPLICATION EXAMPLE

As an example of application, we consider two-qubit quantum gates in an ion chain. With spatial refocusing, we can perform high-fidelity entangling gates even when the Gaussian beam width is comparable with the ion spacing, which significantly simplifies the experimental realization. For two-qubit operations, we need to illuminate only two target ions in the chain. To be concrete, we consider a conditional phase flip (CPF) gate, $U_{jn}^{\mathrm{CPF}} = \exp(i\pi\sigma_j^z\sigma_n^z/4)$, mediated by transverse phonon modes based on the scheme in Refs. [18,19]. Here we only list the essential formula and for detailed derivation we point the readers to the original papers. From a practical point of view, one only needs to
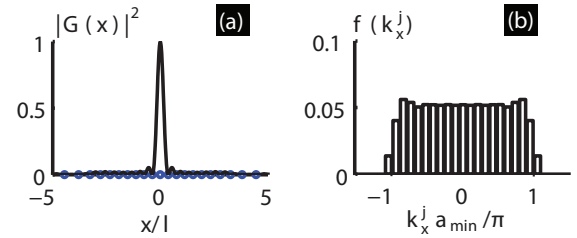

FIG. 2. (Color online) (a) Intensity (amplitude modulus squared) profile of superposition of 21 plane waves with different wave-vector components k_x^j along the chain. Blue circles indicate ions' positions. The unit of position x is $l = (\frac{Z^2 e^2}{4\pi\epsilon_0 M\omega_z^2})^{1/3}$, where Ze and M are the charge and mass of each ion, ϵ_0 is the free space permittivity, and ω_z is the trap frequency along the z axis. (b) Amplitudes of spectral components. Here $a_{\min}$ is the smallest spacing of ions in the middle of the chain.

have Eq. (4) below in hand to understand this example. We define the trap axis to be the z direction. The gate is achieved by applying a state-dependent ac Stark shift on the ions, induced by a pair of Raman beams with frequency detuning μ and wave-vector difference $\Delta\mathbf{k}$ along the transverse direction x. The effective Hamiltonian for the laser-ion interaction is $H = \sum_{j=1}^{N} \hbar\Omega_j \cos(\Delta k \cdot q_j + \mu t)\sigma_j^z$, where q_j is the jth ion's displacement operator along the x direction and σ_j^z acts on the qubit space of the jth ion. Expanding q_j with normal phonon modes [20] $q_j = \sum_k b_j^k \sqrt{\hbar/2M\omega_k}(a_k + a_k^\dagger)$ and assuming the Lamb-Dicke regime $\eta_k = |\Delta k|\sqrt{\hbar/2M\omega_k} \ll 1$, the interaction picture Hamiltonian under the rotating wave approximation is $H_I = -\sum_{j,k=1}^{N} \hbar\chi_j(t)g_j^k(a_k^\dagger e^{i\omega_k t} + a_k e^{-i\omega_k t})\sigma_j^z$, where $g_j^k = \eta_k b_j^k$, $\chi_j(t) = \Omega_j(t)\sin(\mu t)$, b_j^k is the normal-mode wave function, M is the ion mass, and ω_k is the frequency of the kth motional mode. The associated evolution operator is [18,19]

$$U(\tau) = \exp\left(i\sum_j \phi_j(\tau)\sigma_j^z + i\sum_{j<n}\phi_{jn}(\tau)\sigma_j^z\sigma_n^z\right), \quad (4)$$

where

$$\phi_j(\tau) = \sum_k \left(\alpha_j^k(\tau)a_k^\dagger + \mathrm{H.c.}\right),$$

$$\alpha_j^k(\tau) = \int_0^\tau \chi_j(t)g_j^k e^{i\omega_k t}dt,$$

$$\phi_{jn}(\tau) = 2\int_0^\tau dt_2 \int_0^{t_2} dt_1 \sum_k \chi_j(t_2)g_j^k g_n^k \chi_n(t_1)$$

$$\times \sin[\omega_k(t_2 - t_1)].$$

This is the key equation of this gate example so let us give more comments to clarify the picture. The evolution operator contains single-spin and two-spin parts. The coefficients of the single-spin part $\phi_j(\tau)$ are operators acting on the motional degree of freedom. They give ions an internal state dependent displacement of the motion. This would entangle the spin and motional degrees of freedom. Since we care only about the spin part without measuring the motional states, spin-motion entanglement reduces the purity of the spin states. To get a high-fidelity gate we desire a vanishing single-spin part. The coefficients of the two-spin part of evolution $\phi_{jn}(\tau)$ are

c numbers and they only add a phase to the state. Both $\phi_j(\tau)$ and $\phi_{jn}(\tau)$ can be tuned by varying the Raman detuning μ, the gate time τ, and the time-dependent laser Rabi frequency $\Omega_j(t)$. By definition of a controlled phase flip gate between ions j and n, one should have $\phi_{jn}(\tau) = \pi/4$, with every other single-spin and two-spin coefficient being zero. To perform such a gate, we shine lasers to ions j and n only, i.e., $\Omega_i = 0$ for $i \neq j, n$, and optimize over μ so that the effective evolution best approximates U_{jn}^{CPF}. For simplicity, here we assume a time-independent Ω and pick a relatively long gate time, $\tau = 180\tau_0$ ($\tau_0 \equiv 2\pi/\omega_z$ is the trap period). The gate fidelity is quantified by $F = \mathrm{Tr}_m\langle\Psi_f|U(\tau)|\Psi_0\rangle\langle\Psi_0|U^\dagger(\tau)|\Psi_f\rangle$, where $|\Psi_0\rangle = \frac{1}{2}(|0\rangle + |1\rangle) \otimes (|0\rangle + |1\rangle)$ is the assumed initial state, $|\Psi_f\rangle \equiv U_{jn}^{\mathrm{CPF}}|\Psi_0\rangle$ is the ideal final state, and Tr_m indicates tracing over all the motional modes.

Similar to real experiments, we apply Gaussian beams to the target ions j and n. We consider two entangling CPF gates in a 20-ion chain with $\omega_x/\omega_z = 10$, one for two center ions and the other for two ions on one edge, with the beam width about 15% larger than the separation of the two center ions and 2/3 of separation of the two edge ions. The ion spacings and laser beam width are fixed throughout the calculation. Clearly the condition $w/a \ll 1$ is violated in both cases. All the transverse phonon modes are assumed to be initially in thermal states with the same temperature T such that the center-of-mass mode has one phonon on average, a typical situation after Doppler cooling. We scan over the Raman detuning μ and for each μ optimize over Ω_j and Ω_n to find the best possible gate fidelity. As expected, without applying correction beams the fidelity of the gate is rather low [see the top curves in Figs. 3(a) and 3(b)]. However, keeping all other parameters fixed, the gate error is largely reduced by including only one correction beam and including two correction beams the fidelity gets very close to the ideal case. For the center ions, three correction beams on both sides already reduce the gate error by nearly 3 orders of magnitude. As shown in Fig. 3(c), the gate infidelity (t1 fidelity) caused by the crosstalk error decreases exponentially with the number of correction beams, until one approaches the optimal value set by other error sources. Note that with time constants Ω_j and Ω_n, there is an intrinsic gate fidelity due to the lack of control knobs, shown in Fig. 3(c) as dashed lines.

V. EXPERIMENTAL IMPLEMENTATION AND ERROR RESISTANCE

The proposed spatial refocusing technique is ready to implement in many quantum computation architectures, such as harmonically trapped ion crystals [4,21] or arrays of micro-traps [22], Rydberg atoms in optical lattices [23], arrays of optical tweezers [24], etc. After measurement of qubit positions, laser focusing positions, and the laser beam profile, one only needs to apply the inverse linear transformation M_{nj}^{-1} to the target beam profile G_j and use the result as input to the beam delivery device. Removing the need of strong focusing, this scheme should significantly simplify the required optics. Another nice feature is that we do not even require each beam to center at each qubit, as long as the beam positions are known and fixed. The scheme requires coherence between the correction beams. Since Raman beams are used we only need to stabilize the relative phase between the Raman beams. We also note that in small-scale systems, the $\ln(1/\epsilon)$ scaling of the number of required correction beams n_{corr} with the truncation error is often irrelevant. An array of N coherent pulses should always suffice for the generation of arbitrary laser strength profile for N qubits. So one would never need ten beams to address five qubits.

In practice, spatial refocusing is subject to several types of experimental noise. First of all, the ions are not stationary point particles. Their positions fluctuate thermally and quantum mechanically. Second, the amplitudes and phases of each beam in the array may deviate from the prescription. It is unclear whether the interference is robust to these deviations. We first estimate the position fluctuations of the ions. Take a 21-ion chain as an example, the ion spacing varies between 1.02 and 1.78 μm, with the smallest spacing in the middle of the chain. Among the axial motional modes the center-of-mass mode has the lowest frequency, about $2\pi \times 1$ MHz, and the corresponding oscillator length is $\sqrt{\hbar/2M\omega_z} \approx 5.4$ nm. The other axial modes all have higher frequencies and the oscillator lengths are even smaller. Assuming the Doppler cooling limit, i.e., with temperature given by $k_B T = \hbar\Gamma/2$ and the cooling transition linewidth $\Gamma \approx 2\pi \times 20$ MHz, the center-of-mass mode along z contains on average $\frac{k_B T}{\hbar\omega_z} \approx 10$ phonons for a trap with $\omega_z = 2\pi \times 1$ MHz. With these realistic data, the exact
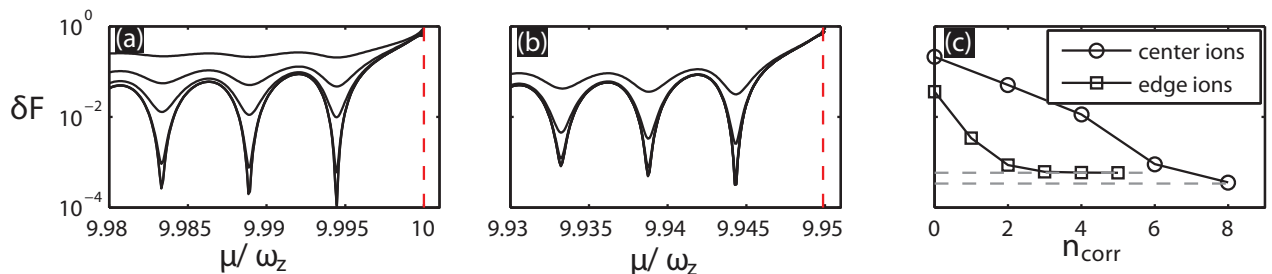

FIG. 3. (Color online) Panels (a) and (b): Infidelity ($\delta F \equiv 1 - F$) of the CPF gate versus the Raman detuning μ for (a) two ions in the center and (b) two ions on one edge in a 20-ion chain. Vertical dashed lines indicate the position of the transverse phonon modes. The beam waist is set to 15% larger than the minimum spacing (at the center) of ions and about 2/3 of the maximum spacing (at the edge) of the chain. In panel (a), curves from top to bottom are for the cases with 0, 2, 4, 6, and 8 correction beams, respectively; in panel (b), curves from top to bottom are for the cases with 0, 1, 2, and 3 correction beams. (c) Infidelity under a fixed Raman detuning $\mu = 9.9888\omega_z$ for center ions and $\mu = 9.9387\omega_z$ for edge ions, as a function of the number of correction beams n_{corr}. Dashed lines denote the infidelity under perfect focusing (with zero crosstalk error).

numerical calculation taking all the axial modes into account shows that for each ion the standard deviation of position ranges from 6.5 to 10 nm, at least 2 orders of magnitude smaller than the interion spacing. So for our purpose here the noise caused the thermal motion of ions is negligible. For the second problem, since the laser beams superpose linearly to give the final refocused pulse, an arbitrary deviation of the jth pulse's amplitude $\delta f(x_j - x_i)$ only adds noise $\delta f(x_j - x_i)g(x - x_j)$ to the final amplitude distribution $G(x - x_i)$. To consider both strength and phase error of the laser, we allow the deviation $\delta f(x_j - x_i)$ to be a complex number. To quantify the effect of $\delta f(x_j - x_i)$, we parametrize the deviation as follows:

$$f(x_j - x_i) + \delta f(x_j - x_i) = f(x_j - x_i)(1 + r_j)\exp(i\phi_j), \tag{5}$$

where the real numbers r_j and ϕ_j measure, respectively, the relative amplitude error and phase error of the beam on ion j. Each r_j/ϕ_j is sampled from the normal distribution with zero mean and standard deviation $\Delta r/\Delta\phi$, i.e., $r_j \sim \mathcal{N}(0,\sigma^2 = \Delta r^2)$ and $\phi_j \sim \mathcal{N}(0,\sigma^2 = \Delta\phi^2)$. We define the quantity

$$\epsilon = \frac{1}{N}\sum_j ||G(x_j - x_i)|^2 - |\tilde{G}(x_j - x_i)|^2| \tag{6}$$

to measure the difference of actual and ideal intensity distribution. We now do a numerical simulation to investigate the robustness of the interference. We take a 21-ion chain harmonically trapped and try to address the central ion, $i = 11$. The ideal target is $G(x_j - x_{11}) = \delta_{j,11}$. Assume the addressing beams have a Gaussian profile with width the same as the distance between the 11th and 12th ion. We randomly sample r_j and ϕ_j 5000 times, calculate ϵ for each sample, and plot the average $\bar{\epsilon}$ as a function of Δr and $\Delta\phi$ (Fig. 4). We find that the interference pattern is pretty robust. For 5% standard amplitude error and 0.2 radians phase error, the average intensity error $\bar{\epsilon}$ is still below 1%. In terms of gate infidelity, we did numerical experiments and found that 1% intensity error induces on the order of 10^{-2} (10^{-3}) infidelity for two center ions with $n_{\text{corr}} = 8$ (edge ions with $n_{\text{corr}} = 5$), with every other parameter the same as described in the caption of Fig. 3. For 0.5% intensity error, both infidelities are on the 10^{-3} level.
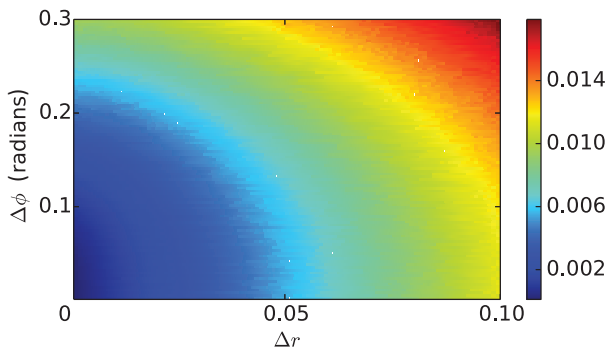

FIG. 4. (Color online) Average intensity error $\bar{\epsilon}$ as a function of standard amplitude/phase error $\Delta r/\Delta\phi$. The color encodes values of $\bar{\epsilon}$. Each point is obtained with 5000 random samples of $r_j \sim \mathcal{N}(0,\sigma^2 = \Delta r^2)$ and $\phi_j \sim \mathcal{N}(0,\sigma^2 = \Delta\phi^2)$.

VI. CONCLUSION

In summary, we have proposed a spatial refocusing technique to achieve effective individual addressing and reduce crosstalk error in a general multiqubit platform. The scheme is efficient as the crosstalk error decreases exponentially with the number of correction beams, and the cost in the laser power is modest even when the beam width is comparable with the qubit separation. The scheme works universally for any type of quantum gate and can apply to any quantum computational platform.

APPENDIX: SOLVING THE ENVELOPE FUNCTION WITH TOEPLITZ MATRIX THEORY

According to the Toeplitz matrix theory, the general solution to the equation $M_{lj}f_{ji} = \delta_{li}$ has the form $f_{ji} = \sum_k c_k^{+/-}(a_k)^{j-i}$, where c_k^+ and c_k^- are for the regions $j > i$ and $j < i$, respectively. Here a_k are the roots of the polynomial $P_n(x) = x^n(1 + \sum_{m=1}^{n}(1/x^m + x^m)\gamma^{m^2})$ and $c_k^{+/-}$ are coefficients to be determined (the bandwidth of the matrix M_{lj} is $2n + 1$). Our first observation is that the roots come in pairs $(a, 1/a)$ due to the symmetry $x \leftrightarrow 1/x$. Thus f_{ji} is composed of terms like $c_k^{+/-}(a_k)^{j-i}$ decaying (increasing) exponentially with $|j - i|$ if $a_k < 1$ ($a_k > 1$). In the region $j > i$ ($j < i$), the boundary condition at $|j - i| \to \infty$ requires $c_k = 0$ for $a_k > 1$ ($a_k > 1$). Note that in the large $|j - i|$ limit, the a_k closest to the unity should dominate since other components die out more quickly. Next we prove that $-\gamma$ (and hence $-1/\gamma$) is a root of $P_n(x)$ when n is sufficiently large:

$$\frac{P_n(-\gamma)}{(-\gamma)^n} = 1 + \sum_{m=1}^{n}(-1)^m\left(\gamma^{m^2+m} + \gamma^{m^2-m}\right)$$

$$= 1 + \sum_{m=1}^{n}(-1)^m\gamma^{m^2+m} + \sum_{m=0}^{n-1}(-1)^{m+1}\gamma^{m^2+m}$$

$$= (-1)^n\gamma^{n^2+n} + \sum_{m=1}^{n-1}(-1)^m(1-1)\gamma^{m^2+m}$$

$$= (-1)^n\gamma^{n^2+n} \to 0, \quad \text{when } n \text{ is large.}$$

The characteristic quantities of $P_n(x)$ are γ, γ^4, γ^9, ..., of which the one closest to the unity is γ. This leads us to conjecture $(-\gamma)$ is the root of $P_n(x)$ closest to 1 in magnitude. This turns out to be true. Since $\tilde{P}_n(x) = P_n(x)/x^n > 0$ when $x > 0$, there is no positive root. Let us focus on the interval $[-1,0)$. For $n = 1$, $\tilde{P}_1(x) = 1 + \gamma(1/x + x)$ is monotonically decreasing from $\tilde{P}_1(-1) = 1 - 2\gamma$ to $\tilde{P}_1(0^-) \to -\infty$ and there is one root in this interval: $\frac{-1+\sqrt{1-4\gamma^2}}{2\gamma} \approx \frac{-1+1-2\gamma^2}{2\gamma} = -\gamma$. When increasing n by 1, we include one more term,

$Q_{n+1}(x) = (1/x^{n+1} + x^{n+1})\gamma^{(n+1)^2}$. Due to the small factor $\gamma^{(n+1)^2}$, the contribution of Q_{n+1} can be comparable with that of Q_n only when $|x| \lesssim \gamma^{2n+1}$. Since $Q_n(0^-)$ approaches $+\infty$ for even n and $-\infty$ for odd n and Q_n is always monotonic on $[-1,0)$, adding one more term always introduces one more turning point in $\tilde{P}_n(x)$ and thus adds one more root with magnitude much smaller than the previous roots. Therefore $(-\gamma)$ is the root with the largest magnitude by far on $[-1,0)$. We therefore conclude $f_{ji} \propto (-\gamma)^{|j-i|}$ when $|j-i|$ is large.

[1] J. P. Home *et al.*, Science **325**, 1227 (2009); M. Anderlini *et al.*, Nature (London) **448**, 452 (2007); J. R. Petta *et al.*, Science **309**, 2180 (2005); M. Steffen *et al.*, *ibid.* **313**, 1423 (2006); L. Isenhower, E. Urban, X. L. Zhang, A. T. Gill, T. Henage, T. A. Johnson, T. G. Walker, and M. Saffman, Phys. Rev. Lett. **104**, 010503 (2010); T. Wilk, A. Gaetan, C. Evellin, J. Wolters, Y. Miroshnychenko, P. Grangier, and A. Browaeys, *ibid.* **104**, 010502 (2010).

[2] L. DiCarlo *et al.*, Nature (London) **460**, 240 (2009); A. Politi *et al.*, Science **325**, 1221 (2009); E. Lucero *et al.*, Nat. Phys. **8**, 719 (2012).

[3] M. D. Reed *et al.*, Nature (London) **482**, 382 (2012); P. Schindler *et al.*, Science **332**, 1059 (2011).

[4] K. Kim *et al.*, Nature (London) **465**, 590 (2010); R. Islam *et al.*, Nat. Commun. **2**, 377 (2011); J. T. Barreiro *et al.*, Nature (London) **470**, 486 (2011); B. P. Lanyon *et al.*, Science **334**, 57 (2011).

[5] M. A. Nielsen and I. L. Chuang, *Quantum Computation and Quantum Information* (Cambridge University Press, Cambridge, UK, 2000).

[6] C. Kim, C. Knoernschild, B. Liu, and J. Kim, IEEE J. Sel. Top. Quantum Electron. **13**, 322 (2007); C. Knoernschild *et al.*, Appl. Phys. Lett. **97**, 134101 (2010).

[7] W. S. Bakr *et al.*, Nature (London) **462**, 74 (2009); J. F. Sherson *et al.*, *ibid.* **467**, 68 (2010).

[8] M. Saffman, Opt. Lett. **29**, 1016 (2004).

[9] G. S. Agarwal and K. T. Kapale, J. Phys. B **39**, 3437 (2006); J. Cho, Phys. Rev. Lett. **99**, 020502 (2007); D. D. Yavuz and N. A. Proite, Phys. Rev. A **76**, 041802(R) (2007); A. V. Gorshkov, L. Jiang, M. Greiner, P. Zoller, and M. D. Lukin, Phys. Rev. Lett. **100**, 093005 (2008); D. Viscor, J. L. Rubio, G. Birkl, J. Mompart, and V. Ahufinger, Phys. Rev. A **86**, 063409 (2012).

[10] J. A. Miles, Z. J. Simmons, and D. D. Yavuz, Phys. Rev. X **3**, 031014 (2013).

[11] C. Weitenberg *et al.*, Nature (London) **471**, 319 (2011).

[12] K. R. Brown, A. W. Harrow, and I. L. Chuang, Phys. Rev. A **70**, 052318 (2004).

[13] Y. Tomita, J. T. Merrill, and K. R. Brown, New J. Phys. **12**, 015002 (2010).

[14] U. Haeberlen, *High Resolution NMR in Solids*, *Selective Averaging*, Advances in Magnetic Resonance Series, Supplement 1 (Academic Press, New York, 1976).

[15] See H. K. Ng, D. A. Lidar, and J. Preskill, Phys. Rev. A **84**, 012305 (2011), and references therein.

[16] W. F. Trench, J. Soc. Ind. Appl. Math. **12**, 515 (1964).

[17] S. Korenblit *et al.*, New J. Phys. **14**, 095024 (2012).

[18] S.-L. Zhu, C. Monroe, and L.-M. Duan, Phys. Rev. Lett. **97**, 050505 (2006).

[19] S.-L. Zhu, C. Monroe, and L.-M. Duan, Europhys. Lett. **73**, 485 (2006).

[20] D. F. V. James, Appl. Phys. B **66**, 181 (1998).

[21] G.-D. Lin *et al.*, Europhys. Lett. **86**, 60004 (2009).

[22] J. D. Siverns *et al.*, New J. Phys. **14**, 085009 (2012); J. M. Amini *et al.*, *ibid.* **12**, 033031 (2010).

[23] M. Saffman, T. G. Walker, and K. Mølmer, Rev. Mod. Phys. **82**, 2313 (2010).

[24] R. Dumke, M. Volk, T. Muther, F. B. J. Buchkremer, G. Birkl, and W. Ertmer, Phys. Rev. Lett. **89**, 097903 (2002); S. Bergamini *et al.*, J. Opt. Soc. Am. B **21**, 1889 (2004).